Cancer Immunology Miniatures

Cancer Immunology Research

Intrinsic Resistance to Immune Checkpoint Blockade in a Mismatch Repair–Deficient Colorectal Cancer

Carino Gurjao[1,2], David Liu[1,2], Matan Hofree[2], Saud H. AlDubayan[1,2], Isaac Wakiro[3], Mei-Ju Su[4], Kristen Felt[5], Evisa Gjini[5], Lauren K. Brais[1], Asaf Rotem[3], Michael H. Rosenthal[6], Orit Rozenblatt-Rosen[2], Scott Rodig[5,7], Kimmie Ng[1], Eliezer M. Van Allen[1,2,3], Steven M. Corsello[1,2], Shuji Ogino[2,8,9,10], Aviv Regev[2], Jonathan A. Nowak[8,9], and Marios Giannakis[1,2]

Abstract

Immunotherapy with checkpoint inhibitors, such as the programmed death-1 (PD-1) antibodies pembrolizumab and nivolumab, are effective in a variety of tumors, yet not all patients respond. Tumor microsatellite instability-high (MSI-H) has emerged as a biomarker of response to checkpoint blockade, leading to the tissue agnostic approval of pembrolizumab in MSI-H cancers. Here we describe a patient with MSI-H colorectal cancer that was treated with this immune checkpoint inhibitor and exhibited progression of disease. We examined this intrinsic resistance through genomic, transcriptional, and pathologic characterization of the patient's tumor and the associated immune microenvironment. The tumor had typical MSI-H molecular features, including a high neoantigen load. We also identified biallelic loss of the gene for β_2-microglobulin (*B2M*), whose product is critical for antigen presentation. Immune infiltration deconvolution analysis of bulk transcriptome data from this anti-PD-1–resistant tumor and hundreds of other colorectal cancer specimens revealed a high natural killer cell and M2 macrophage infiltration in the patient's cancer. This was confirmed by single-cell transcriptome analysis and multiplex immunofluorescence. Our study provides insight into resistance in MSI-H tumors and suggests immunotherapeutic strategies in additional genomic contexts of colorectal cancer.

Introduction

Immune checkpoint inhibitors, such as programmed cell death-1 (PD-1, *PDCD1*) antibodies, have revolutionized cancer treatment by demonstrating long-lasting responses in patients with several types of malignancies (1). However, only a subset of patients experience benefit from these agents and complete response remains uncommon. In this context, tumor DNA mismatch repair deficiency (dMMR) and a high level of microsatellite instability (MSI-H) have emerged as powerful genomic markers of response to immune checkpoint inhibitors across malignancies (2, 3), leading to the tissue agnostic FDA approval of the PD-1 antibody, pembrolizumab, in refractory dMMR/MSI-H solid malignancies and to the approval of the PD-1 antibody nivolumab with or without the CTLA-4 antibody ipilimumab in dMMR/MSI-H colorectal cancer after fluoropyrimidine-, oxaliplatin-, and irinotecan-based chemotherapy. The leading proposed reason for the immunogenicity of dMMR tumors is their high mutational and neoantigen burden (4); however, only 30% to 55% of patients with such cancers respond to immune checkpoint blockade with another 10% to 28% of patients remaining primarily refractory to immunotherapy (2, 3, 5, 6). To date, the molecular and microenvironmental features of dMMR/MSI-H tumors that are intrinsically resistant to immune checkpoint blockade remain unknown. Their characterization could provide insights for novel combination immunotherapies in this subset of tumors and also inform resistance, and strategies to overcome it, in additional genomic contexts.

Here, we describe a patient with metastatic dMMR colorectal cancer who was treated with pembrolizumab after combination chemotherapy. Despite having confirmed dMMR/MSI-H status and a high neoantigen load, her disease progressed on pembrolizumab. To analyze the basis of this intrinsic immune checkpoint inhibitor resistance, we performed bulk

[1]Department of Medical Oncology, Dana-Farber Cancer Institute and Harvard Medical School, Boston, Massachusetts. [2]Broad Institute of MIT and Harvard, Cambridge, Massachusetts. [3]The Center for Cancer Precision Medicine, Dana-Farber Cancer Institute, Boston, Massachusetts. [4]Biotherapeutic and Medicinal Sciences, Biogen, Cambridge, Massachusetts. [5]Center for Immuno-Oncology, Dana-Farber Cancer Institute, Boston, Massachusetts. [6]Department of Radiology, Dana-Farber Cancer Institute, Brigham and Women's Hospital, and Harvard Medical School, Boston, Massachusetts. [7]Department of Pathology, Brigham and Women's Hospital, Boston, Massachusetts. [8]Department of Oncologic Pathology, Dana-Farber Cancer Institute and Harvard Medical School, Boston, Massachusetts. [9]Program in MPE Molecular Pathological Epidemiology, Department of Pathology, Brigham and Women's Hospital and Harvard Medical School, Boston, Massachusetts. [10]Department of Epidemiology, Harvard T.H. Chan School of Public Health, Boston, Massachusetts.

Note: Supplementary data for this article are available at Cancer Immunology Research Online (http://cancerimmunolres.aacrjournals.org/).

Corresponding Author: Marios Giannakis, Dana-Farber Cancer Institute, 450 Brookline Ave., Boston, MA 02115. Phone: 617-582-7263; Fax: 617-632-5370; E-mail: Marios_Giannakis@dfci.harvard.edu

Cancer Immunol Res 2019;7:1230–6

doi: 10.1158/2326-6066.CIR-18-0683

and single-cell characterization of her tumor and the associated immune microenvironment.

Materials and Methods

Patient study

The patient provided written consent to participate in research protocols for additional core biopsies and research testing. All biopsies and molecular testing were performed in accordance with protocols approved by the Institutional Review Board at the Dana-Farber Cancer Institute (Boston, MA).

Statistical analyses

We used R-3.4.4 to perform statistical analyses. For two-group comparisons, significance was evaluated by the Mann–Whitney *U* test for nonnormal distributions, and with a two-tailed student *t* test otherwise. $P < 0.05$ was considered statistically significant.

Bulk sequencing

DNA and RNA extractions from formalin-fixed, paraffin-embedded (FFPE) sections and peripheral blood were carried out using standard methods (7). Whole-exome sequencing (WES) was performed as detailed previously (8) on the pre-immunotherapy tumor and peripheral blood, with mean depth of coverage of 270× and 101×, respectively. For bulk whole-transcriptome sequencing (RNA-seq), we used the TCap protocol (Transcriptome Capture, as described on genomics.broadinstitute.org/products/whole-transcriptome-sequencing), which is optimal for low input and degraded samples such as FFPE samples. Using this method, RNA-seq was performed on the pretreatment tumor with >22,000 genes and 99.4% exons detected.

Single-cell sequencing

The core biopsy was received in additive-free M199 Media (Thermo Fisher Scientific catalog no. 11150059). To generate a cell suspension for single-cell RNA-seq (scRNA-seq), the core was minced into smaller approximately 1-mm pieces, which were then dissociated by a combination of mechanical and enzymatic digestion with Accumax (Innovative Cell Technologies catalog no. AM105) at room temperature for 10 minutes. Following dissociation, cells were strained through a 100-μm strainer, washed with ice-cold PBS (Ca/Mg free) with 2% FCS, and resuspended in 0.04% BSA (Thermo Fisher Scientific catalog no. AM2616) with PBS. From this suspension, two channels were loaded on 10×; one with 4,000 cells and the other with 6,000 cells. Libraries were prepared using established protocols. Droplet-based massively parallel scRNA-seq was performed using Chromium Single-Cell 3′ Reagents Kits (v.1) according to the manufacturer's protocols (10x Genomics). The generated scRNA-seq libraries were sequenced using 100 cycle Illumina HiSeq. After quality control, 595 resulting cells were used for further analyses.

Variant calling

Tumor somatic mutations were called from WES using standardized pipelines including MuTect for somatic SNV inference and Strelka for small insertion/deletions. We corrected for FFPE and oxoguanine artifacts, and used a panel of normal filter as described previously (9).

Tumor purity and ploidy were inferred using ABSOLUTE, and cancer cell fraction (CCF) of mutations (i.e., the proportion of tumor cells with the mutation) estimated. Allelic copy-number alterations were inferred using an adaptation of a circular binary segmentation (10) and corrected for tumor purity and ploidy. The mutations discussed in this work were orthogonally validated by a next-generation CLIA-certified sequencing panel (11). To study the mutational signatures in the tumor of the patient, we used DeconstructSig based on linear combination analysis of preexisting signatures. POLYSOLVER was used to detect the human leukocyte antigen (HLA) type of the patient, which enabled neoantigen prediction using NetMHCpan as described previously (9).

MLH1 methylation testing

DNA methylation patterns in the CpG island of the MLH1 promoter gene were determined by chemical (bisulfite) modification of unmethylated cytosines to uracil and subsequent PCR using primers specific for either methylated or the modified unmethylated DNA (12). The PCR products were analyzed by capillary gel electrophoresis.

Gene expression analysis

For bulk RNA-seq analysis, STAR and RSEM were used for alignment and gene expression quantification, respectively. Immune cell subset deconvolution was performed using CIBERSORT to assess the relative and total abundance of 22 immune cell types. For single-cell analysis, gene expression counts were obtained by aligning reads to the GRCh38 genome using the Cell Ranger analysis pipeline (https://support.10xgenomics.com/single-cell-gene-expression/software/release-notes/2-1). The consensus molecular subtypes (CMS; ref. 13) were called using the "CMScaller" R package.

Immunohistochemistry and multiplex immunofluorescence

Tumor sections were deparaffinized and stained for β_2-microglobulin (polyclonal rabbit anti-human β_2-microglobulin, Dako A007202-2) and MMR proteins (as described in ref. 14) with standard immunohistochemistry (IHC) protocols. Staining for multispectral imaging analysis was performed on a BOND RX Automated Stainer (Leica Biosystems) utilizing 5-μm thick section of FFPE tissue. After deparaffinization, rehydration, and antigen retrieval, slides were serially stained with primary antibodies to Cytokeratin (clone AE1/AE3, DAKO), CD3 (polyclonal, Dako A0452), and CD56 (clone 123C3; Dako), followed by incubation with an anti-rabbit polymeric horseradish peroxidase secondary IgG (BOND Polymer Refine Detection Kit, Leica Biosystems). Signal for antibody complexes was labeled and visualized by Opal Fluorophore Reagents (PerkinElmer). Image acquisition was performed using the Mantra Multispectral Imaging Platform (Vectra 3.0, PerkinElmer). Representative intratumoral regions of interest were chosen by a gastrointestinal pathologist (J.A. Nowak), and 3 to 5 fields of view (FOV) were acquired at 20× resolution as multispectral images. Cell identification was performed as described previously (15). In short, after image capture, the FOV were spectrally unmixed and then analyzed using supervised machine learning algorithms within Inform 2.3 (PerkinElmer). Immune cell densities were then calculated based upon phenotyped cell counts and tissue areas.

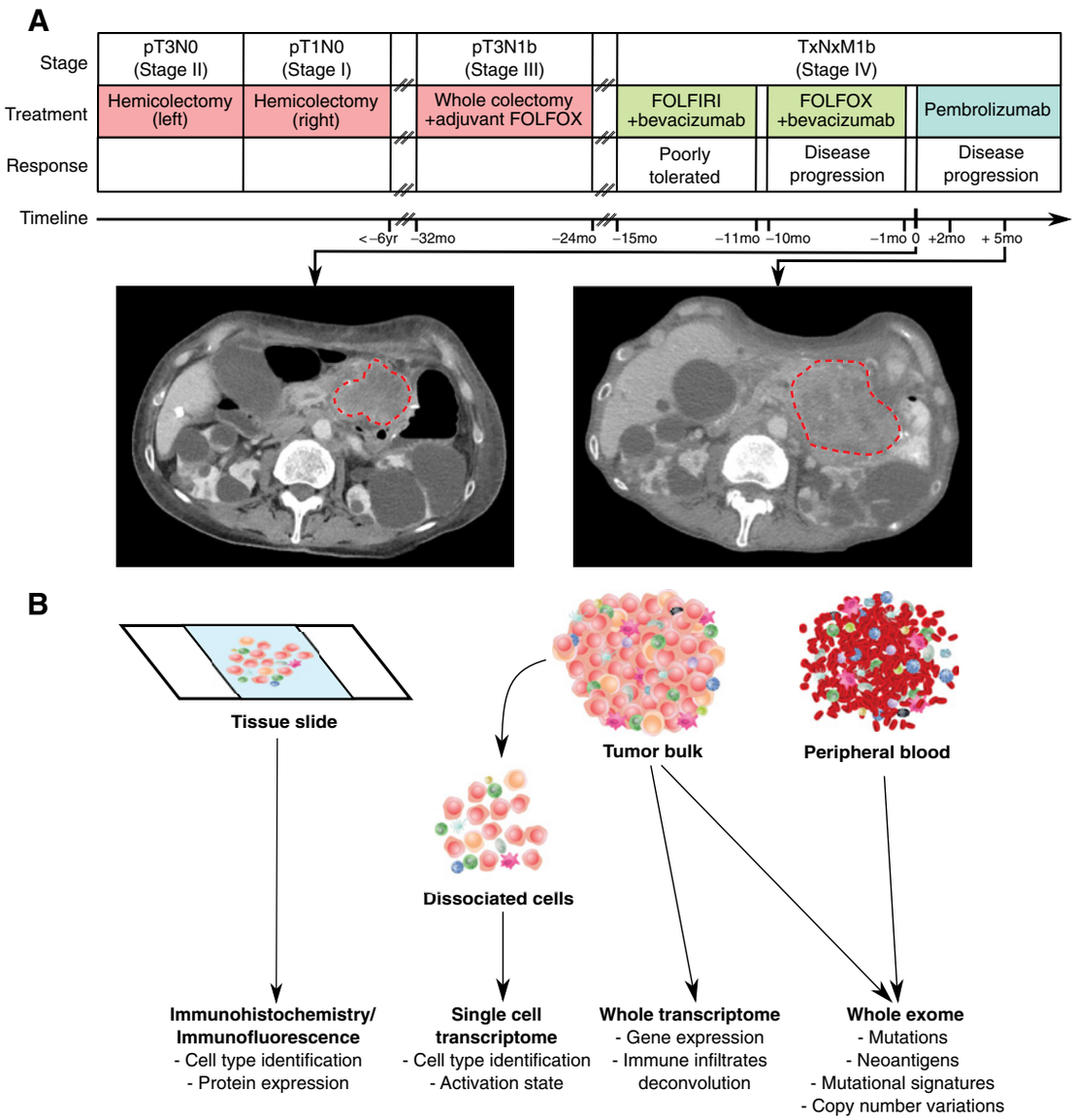

Figure 1.

A, Patient disease and treatment course. The stage, treatments, and response of the patient's cancer are shown. Timepoint zero in the event timeline indicates the start of immunotherapy. CT scans at the indicated timepoints are shown at the bottom. Dotted lines delineate the tumor. **B,** Flowchart of specimens used, data generated, and analyses performed.

Results

Case history

A 78-year-old woman with metastatic colon adenocarcinoma was admitted to the hospital with abdominal pain. CT imaging revealed a large heterogeneously enhancing paracolic mass (Fig. 1A). The patient had a history of three metachronous early-stage colon adenocarcinomas: a stage II (pT3N0) descending colon primary, a stage I (pT1N0) ascending colon primary, and a stage III (pT3N1b) transverse colon primary. She previously underwent sequential left hemicolectomy, right hemicolectomy, and completion colectomy over a 6-year period. Molecular testing of her stage III tumor had showed a *BRAF* c.1799T>A (p.V600E) mutation and loss of MMR proteins MLH1 and PMS2 by IHC. Following her completion colectomy, she received 12 cycles of adjuvant 5-fluorouracil, leucovorin, and oxaliplatin (FOLFOX). However, 1 year later she had disease recurrence in the upper abdominal mesentery and went on to receive 5-fluorouracil, leucovorin, and irinotecan with bevacizumab for metastatic colorectal cancer. She tolerated this poorly and was changed to FOLFOX and bevacizumab with subsequent progression of disease after several months of treatment.

Biopsy of the recurrent tumor was recommended to confirm dMMR and MSI-H status. Ultrasound-guided abdominal mass biopsy was performed. Pathology revealed poorly differentiated

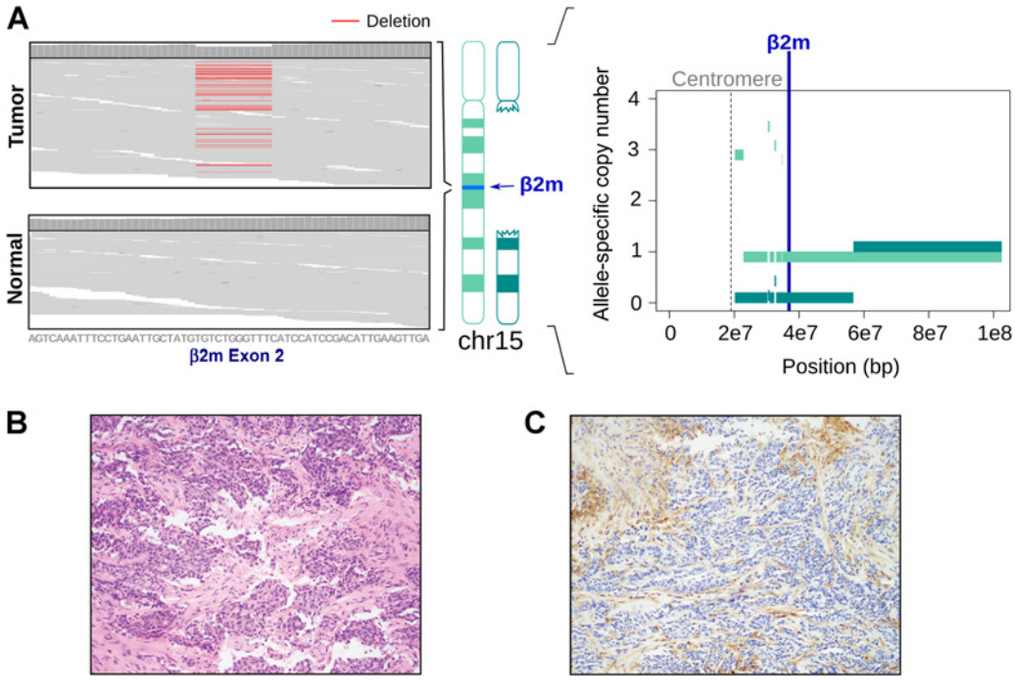

Figure 2.

Impairment of the antigen presentation machinery through biallelic loss of β_2-microglobulin. **A,** Mutation analysis results. The left schematic shows the Integrated Genomics Viewer (IGV) panels of both tumor and normal tissue. Deleted regions are shown in red. The figure on the right shows the allele-specific copy-number profile: the *y* axis represents the copy number of the allele, and the *x* axis shows the genomic localization on chromosome 15. The left figure shows the frameshift deletion in exon 2 of *B2M*, whereas the right figure shows the LOH of a segment of 15q surrounding *B2M*. **B,** Hematoxylin and eosin staining of tumor. **C,** B2M expression. There is complete loss of expression of membranous B2M in tumor cells, with retained expression in surrounding nonneoplastic stromal cells.

adenocarcinoma with loss of nuclear MLH1 and PMS2 staining by IHC, MSI in five of the five genomic markers tested, and methylation of the MLH1 promoter. She was started on pembrolizumab (200 mg every 3 weeks) with restaging scans after 2 months interpreted as progression of disease. Given the possibility of pseudoprogression with immunotherapy, the patient was maintained on therapy, but another set of scans after 5 months of treatment showed clear disease progression (Fig. 1A).

Mutation, copy number, and neoantigen analyses

To investigate for mechanisms of intrinsic resistance to immune checkpoint blockade in this dMMR tumor, we performed preimmunotherapy tumor and matched normal WES, IHC, and multiplex immunofluorescence pathologic analyses, as well as bulk and scRNA-seq (Fig. 1B). WES revealed a high mutation load with a total of 1,857 somatic single-nucleotide variants and small indels (Supplementary Table S1), a high neoantigen load and a quiet copy number landscape (Supplementary Fig. S1A and S1B), as typical for dMMR/MSI-H colorectal cancer (16). Mutational signature analysis demonstrated that the majority of mutations were stemming from a mutational signature associated with dMMR (ref. 17; Supplementary Fig. S1C).

WES also confirmed the presence of a *BRAF* c.1799T>A (p.V600E) mutation, as well as mutations in *RNF43*, a gene that is mutated in approximately 50% of MSI-H colorectal cancers (8). To evaluate the possibility of an inherited cancer risk allele in this patient with a history of multiple tumors, germline coding variants in 14 established colorectal cancer risk genes, as well as 40 cancer risk genes that are part of the DNA repair machinery (Supplementary Table S2) were called and evaluated for pathogenicity as described previously (18). Our assessment showed no known pathogenic or likely pathogenic germline mutations in neither the colorectal cancer risk gene set nor the DNA repair set. There was also no germline MLH1 promoter methylation. Thus, to the best of our current knowledge, the tumor appears to be sporadic.

The patient's tumor harbored a *B2M* frameshift deletion p.V47Afs*6 (CCF = 0.76) and had loss of heterozygosity (CCF = 0.97). The inactivation of *B2M* in this tumor is consistent with a clonal event in its evolution (Fig. 2A). To validate B2M loss, we performed IHC on the preimmunotherapy tumor sample for B2M and confirmed complete loss of expression in the tumor cells (Fig. 2B and C). There were no biallelic inactivation events in other genes of the antigen presentation machinery/IFNγ pathway (*JAK1*, *JAK2*, *STAT1*, *STAT2*, *STAT3*, *CD274*, *PDCD1*, *PDCD1LG2*, *HLA-A*, *HLA-B*, *HLA-C*, *TAP1*, *TAP2*, *IFNGR1*, and *IFNGR2*).

Gene expression and infiltrating immune cell deconvolution

To characterize the tumor's transcriptional state, as well as the tumor–immune microenvironment in this intrinsically resistant dMMR colorectal cancer, we performed bulk RNA-seq (Supplementary Table S1) and compared the results to transcriptional profiles of 594 The Cancer Genome Atlas (TCGA) colorectal cancers that are publicly available on cBioPortal (www.cbioportal.org/, version: coadread_tcga_pan_can_atlas_2018). Subtyping efforts in

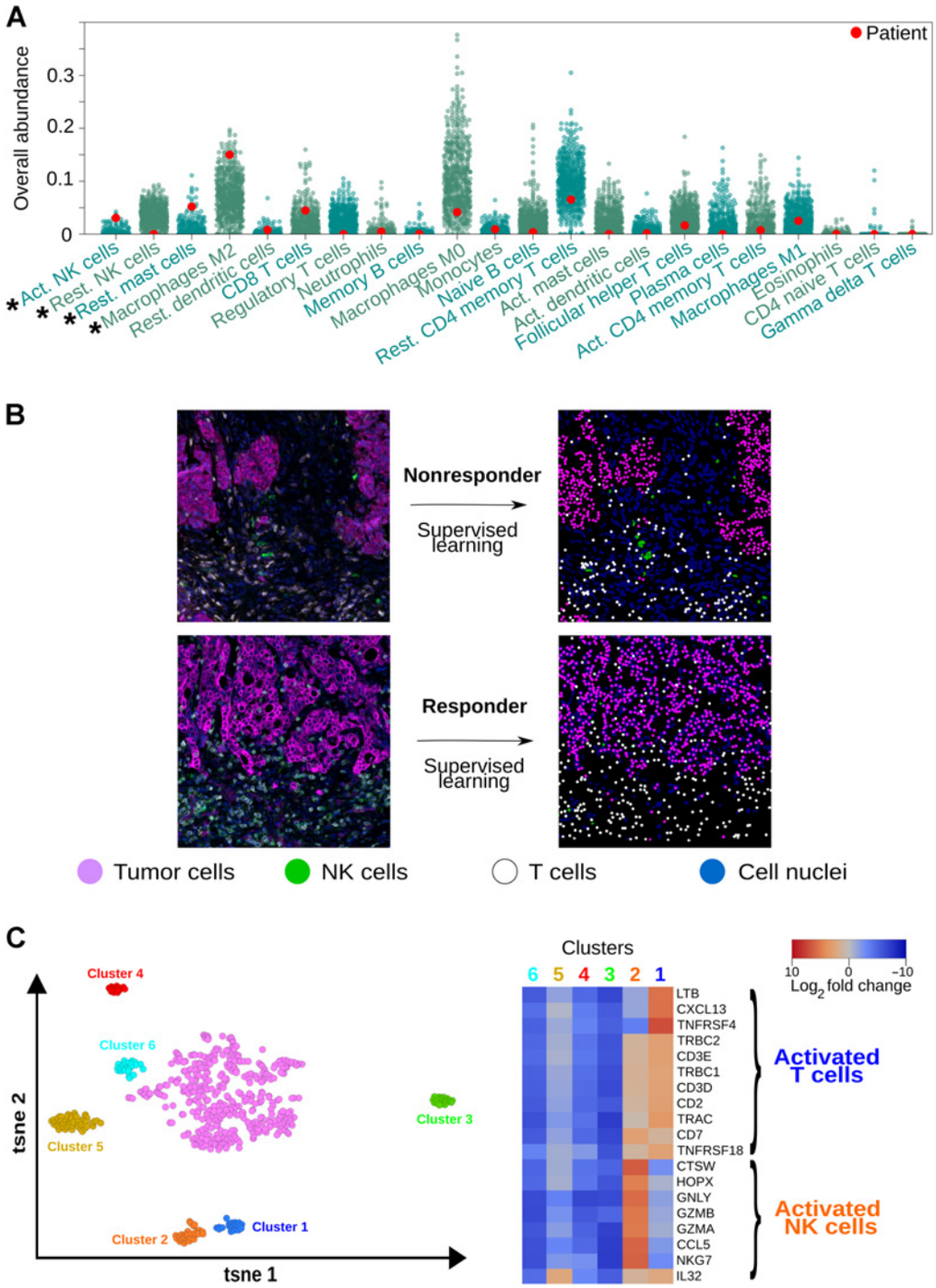

Figure 3.

NK cell infiltration in the tumor–immune microenvironment. **A,** Immune infiltrates deconvolution from RNA-seq data. The immune infiltrates abundances, as a total cell fraction, of the immune checkpoint–resistant tumor (red point) are compared with 594 other colorectal cancer tumors from TCGA. The immune infiltrates (*x* axis) were sorted by *P* values from left to right. The immune infiltrates for which the patient was in the top or bottom 5% are denoted with an asterisk. **B,** Multiplexed immunofluorescence imaging analysis of the tumor–immune microenvironment. Left panels, representative immunofluorescent expression of CD3 (white), CD56 (green), cytokeratin (purple), and DAPI (blue, marking nuclei). Right panels, results from image analysis, driven by machine learning, that identifies $CD3^{+}CD56^{-}$ T cells (white dots) and $CD3^{-}CD56^{+}$ NK cells (green dots) within tumor regions. **C,** Single-cell transcriptional analysis of the tumor. t Distributed Stochastic Neighbor Embedding (t-SNE) visualization (left) of the scRNA-seq data from 595 cells. The heatmap (right) shows significantly differentially expressed genes of interest between the nonepithelial cell clusters.

colorectal cancer have showed the existence of four distinct CMS groups, based on gene expression data (13). As expected, RNA-seq–based CMS classification of this patient's tumor showed a CMS1 gene expression pattern that is typical of MSI-H tumors (13). We also employed RNA-seq immune cell subset deconvolution and found that the patient's tumor had a high inferred immune infiltrate abundance compared with other colorectal cancers from TCGA (within top 2%), as expected given MSI-H status, but also had a significantly higher infiltration with activated natural killer (NK) cells and M2 macrophages (Fig. 3A). These results held true when we restricted the comparison to MSI-H ($n = 73$; Supplementary Fig. S2A) or advanced (stage III and IV) tumors ($n = 240$; Supplementary Fig. S2B). Among the 12 colorectal cancers that were MSI-H with an advanced stage, the tumor of the reported patient had the highest infiltration of both activated NK cells and M2 macrophages. We did not further stratify tumors by *B2M* status, as biallelic inactivation of *B2M* was not validated by IHC in TCGA.

Tumor–immune microenvironment at a single-cell resolution

To orthogonally validate the above findings, we performed multiplex immunofluorescence to quantify T cells [$CD3^+CD56(NCAM1)^-$] and NK cells [$CD3^-CD56(NCAM1)^+$] in the tumor microenvironment (Fig. 3B) and compared the results from this intrinsically resistant tumor to an dMMR/MSI-H tumor from another patient with metastatic colorectal cancer that responded to pembrolizumab. This was a 70-year-old woman who had been previously treated with surgery and FOLFOX/bevacizumab chemotherapy prior to receiving nivolumab and showing response by imaging and tumor marker. We found that there was a higher number of intraepithelial NK cells within the center of the PD-1–resistant cancer [17.4 cells/mm^2 ($\pm$5.6) in the resistant tumor and 1.4 cells/mm^2 ($\pm$1.4) in the responding tumor, $P = 0.032$, two-tailed student t test]. There were no significant differences in T-cell infiltration. To further assess the presence of NK cells in this intrinsically resistant tumor, and to specifically interrogate the transcriptional activation state of these immune cells, we performed single-cell analysis of the precheckpoint inhibition specimen using scRNA-seq. Our results confirm the presence of activated NK cells in this tumor and high expression of activated NK cell markers including *NKG7*, *GZMB*, *GZMA*, and *GNLY* (Fig. 3C).

Discussion

This patient with dMMR/MSI-H colorectal cancer was treated with pembrolizumab but exhibited primary resistance to immune checkpoint blockade with progression of her disease on restaging scans. Her tumor had a high neoantigen load, a mutational signature consistent with dMMR, *BRAF* and *RNF43* mutations, and other molecular features typical of dMMR tumors. On WES prior to initiation of pembrolizumab, we identified somatically acquired biallelic loss of *B2M*, a critical component of the antigen presentation machinery and MHC class I expression. The second hit in this locus was due to loss of heterozygosity, despite an expected overall low copy-number alteration burden. This was consistent with our work describing enrichment of inactivating antigen presentation machinery mutations in MSI-H primary colorectal cancers (19). We confirmed complete loss of B2M protein expression through IHC. Loss of *B2M* has been previously implicated in acquired resistance in melanoma, lung cancer, and MSI-H colorectal cancer (3, 20, 21) and intrinsic resistance in melanoma (22), but it has not been previously described as source of intrinsic resistance in dMMR tumors. This case suggests that MHC class I and B2M expression may need to be considered prior to initiation of PD-1 inhibition to identify patients with dMMR/MSI-H cancers who may not respond to therapy.

To further elucidate the tumor–immune microenvironment, we performed bulk and single-cell transcriptomic analysis. We found that this tumor had the highest inferred activated NK cell and M2 macrophage infiltration when compared with hundreds of colorectal cancer specimens from the TCGA with available bulk transcriptional data. We validated these findings through multiplex immunofluorescence against T cell and NK cell markers and demonstrated enrichment of NK cells in the intrinsically resistant MSI-H tumor compared with one that responded to PD-1 inhibition. We also identified transcriptionally activated NK cells in this immune checkpoint–resistant tumor through scRNA-seq analysis of the tumor and tumor-associated immune cells from the preimmunotherapy biopsy specimen.

NK cells can recognize and eliminate cells lacking MHC class I expression (23, 24), but are also continuously tuned by classical and nonclassical MHC class I molecules, in addition to MHC I–independent mechanisms that instruct NK cells to acquire appropriate missing self-recognition capacity, a process termed NK cell "education" (25, 26). This could at least partially explain the lack of NK cell–mediated tumor control/elimination in a completely B2M-deficient tumor microenvironment, despite an otherwise activated NK cell phenotype. In addition, M2 macrophages have been shown to exert an immunosuppressive role, in particular by impairing NK cells degranulation during cancer progression (27).

These findings suggest that NK cell–based immunotherapies, such as the transfer of "educated" NK cells to patients, could offer an attractive option for MSI-H tumors that are resistant to immune checkpoint inhibition due to lack of antigen presentation. Our findings also further support the development of immunotherapeutic strategies that aim to shift the balance between M2 and M1 macrophages (28, 29). More broadly, our results have implications for primary resistance to immune checkpoint blockade and novel immunotherapeutic approaches through modulation of the innate immune response in patients with cancer.

Disclosure of Potential Conflicts of Interest

A. Rotem is a consultant at, has ownership interest (including stock, patents, etc.) in, and is a consultant/advisory board member for Celsius Therapeutics. S. Rodig reports receiving commercial research grants from Bristol-Myers Squibb, Merck, and KITE/Gilead. K. Ng reports receiving commercial research grants from Genentech, Gilead Sciences, Tarrex Biopharma, Trovagene, Celgene, and Pharmavite and is a consultant/advisory board member for Bayer, Lilly, Seattle Genetics, and Tarrex Biopharma. E.M. Van Allen reports receiving commercial research grants from Novartis and Bristol-Myers Squibb, has ownership interest (including stock, patents, etc.) in Syapse, Genome Medical, Tango Therapeutics, and Microsoft, and is a consultant/advisory board member for Genome Medical, Invitae, Tango Therapeutics, Dynamo, and Illumina. S.M. Corsello reports receiving a commercial research grant from Bayer. A. Regev has ownership interest (including stock, patents, etc.) in Celsius Therapeutics and is a consultant/advisory board member for Thermo Fisher Scientific and Syros Pharmaceuticals. M. Giannakis reports receiving a commercial research grant from Bristol-Myers Squibb and has received advisory board honorarium from AstraZeneca. No potential conflicts of interest were disclosed by the other authors.

Authors' Contributions

Conception and design: D. Liu, O. Rozenblatt-Rosen, S. Rodig, S.M. Corsello, S. Ogino, M. Giannakis

Development of methodology: C. Gurjao, D. Liu, A. Rotem, O. Rozenblatt-Rosen, J.A. Nowak

Acquisition of data (provided animals, acquired and managed patients, provided facilities, etc.): I. Wakiro, M.-J. Su, E. Gjini, L.K. Brais, M.H. Rosenthal, O. Rozenblatt-Rosen, K. Ng, E.M. Van Allen, S.M. Corsello, A. Regev, J.A. Nowak, M. Giannakis
Analysis and interpretation of data (e.g., statistical analysis, biostatistics, computational analysis): C. Gurjao, D. Liu, M. Hofree, S.H. AlDubayan, K. Felt, M.H. Rosenthal, O. Rozenblatt-Rosen, S. Rodig, K. Ng, E.M. Van Allen, S. Ogino, A. Regev, J.A. Nowak, M. Giannakis
Writing, review, and/or revision of the manuscript: C. Gurjao, D. Liu, M. Hofree, S.H. AlDubayan, L.K. Brais, M.H. Rosenthal, O. Rozenblatt-Rosen, S. Rodig, K. Ng, E.M. Van Allen, S.M. Corsello, S. Ogino, J.A. Nowak, M. Giannakis
Administrative, technical, or material support (i.e., reporting or organizing data, constructing databases): C. Gurjao, L.K. Brais, K. Ng, M. Giannakis
Study supervision: O. Rozenblatt-Rosen, K. Ng, M. Giannakis

Acknowledgments

M. Giannakis and this research was supported by a Conquer Cancer Foundation of ASCO Career Development Award, the Project P-Fund, the Cancer Research UK C10674/A27140 Grand Challenge Award, and a Stand Up to Cancer Colorectal Cancer Dream Team Translational Research Grant (grant no. SU2C-AACR-DT22-17). Stand Up to Cancer is a division of the Entertainment Industry Foundation. Research grants are administered by the American Association for Cancer Research, a scientific partner of SU2C. This work was also supported by NIH grants RO1 CA205406 (to K. Ng) and P50 CA127003 (to M. Giannakis).

Received September 28, 2018; revised February 13, 2019; accepted June 12, 2019; published first June 19, 2019.

References

1. Topalian SL, Hodi FS, Brahmer JR, Gettinger SN, Smith DC, McDermott DF, et al. Safety, activity, and immune correlates of anti-PD-1 antibody in cancer. N Engl J Med 2012;366:2443–54.
2. Le DT, Uram JN, Wang H, Bartlett BR, Kemberling H, Eyring AD, et al. PD-1 blockade in tumors with mismatch-repair deficiency. N Engl J Med 2015; 372:2509–20.
3. Le DT, Durham JN, Smith KN, Wang H, Bartlett BR, Aulakh LK, et al. Mismatch repair deficiency predicts response of solid tumors to PD-1 blockade. Science 2017;357:409–13.
4. Giannakis M, Mu XJ, Shukla SA, Qian ZR, Cohen O, Nishihara R, et al. Genomic correlates of immune-cell infiltrates in colorectal carcinoma. Cell Rep 2016;15:857–65.
5. Overman MJ, McDermott R, Leach JL, Lonardi S, Lenz HJ, Morse MA, et al. Nivolumab in patients with metastatic DNA mismatch repair-deficient or microsatellite instability-high colorectal cancer (CheckMate 142): an open-label, multicentre, phase 2 study. Lancet Oncol 2017;18: 1182–91.
6. Overman MJ, Lonardi S, Wong KYM, Lenz HJ, Gelsomino F, Aglietta M, et al. Durable clinical benefit with nivolumab plus ipilimumab in DNA mismatch repair-deficient/microsatellite instability-high metastatic colorectal cancer. J Clin Oncol 2018;36:773–9.
7. Van Allen EM, Wagle N, Stojanov P, Perrin DL, Cibulskis K, Marlow S, et al. Whole-exome sequencing and clinical interpretation of formalin-fixed, paraffin-embedded tumor samples to guide precision cancer medicine. Nat Med 2014;20:682–8.
8. Giannakis M, Hodis E, Jasmine Mu X, Yamauchi M, Rosenbluh J, Cibulskis K, et al. RNF43 is frequently mutated in colorectal and endometrial cancers. Nat Genet 2014;46:1264–6.
9. Miao D, Margolis CA, Gao W, Voss MH, Li W, Martini DJ, et al. Genomic correlates of response to immune checkpoint therapies in clear cell renal cell carcinoma. Science 2018;359:801–6.
10. Olshen AB, Venkatraman ES, Lucito R, Wigler M. Circular binary segmentation for the analysis of array-based DNA copy number data. Biostatistics 2004;5:557–72.
11. Garcia EP, Minkovsky A, Jia Y, Ducar MD, Shivdasani P, Gong X, et al. Validation of OncoPanel: a targeted next-generation sequencing assay for the detection of somatic variants in cancer. Arch Pathol Lab Med 2017;141: 751–8.
12. Grady WM, Rajput A, Lutterbaugh JD, Markowitz SD. Detection of aberrantly methylated hMLH1 promoter DNA in the serum of patients with microsatellite unstable colon cancer. Cancer Res 2001;61:900–2.
13. Guinney J, Dienstmann R, Wang X, de Reyniès A, Schlicker A, Soneson C, et al. The consensus molecular subtypes of colorectal cancer. Nat Med 2015;21:1350–6.
14. Nowak JA, Yurgelun MB, Bruce JL, Rojas-Rudilla V, Hall DL, Shivdasani P, et al. Detection of mismatch repair deficiency and microsatellite instability in colorectal adenocarcinoma by targeted next-generation sequencing. Mol Diagn 2017;19:84–91.
15. Carey CD, Gusenleitner D, Lipschitz M, Roemer MGM, Stack EC, Gjini E, et al. Topological analysis reveals a PD-L1-associated microenvironmental niche for Reed-Sternberg cells in Hodgkin lymphoma. Blood 2017;130:2420–30.
16. Cancer Genome Atlas Network. Comprehensive molecular characterization of human colon and rectal cancer. Nature 2012;487:330–7.
17. Alexandrov LB, Nik-Zainal S, Wedge DC, Aparicio SA, Behjati S, Biankin AV, et al. Signatures of mutational processes in human cancer. Nature 2013; 500:415–21.
18. AlDubayan SH, Giannakis M, Moore ND, Han GC, Reardon B, Hamada T, et al. Inherited DNA-repair defects in colorectal cancer. Am J Hum Genet 2018;102:401–14.
19. Grasso CS, Giannakis M, Wells DK, Hamada T, Mu XJ, Quist M, et al. Genetic mechanisms of immune evasion in colorectal cancer. Cancer Discov 2018;8:730–49.
20. Zaretsky JM, Garcia-Diaz A, Shin DS, Escuin-Ordinas H, Hugo W, Hu-Lieskovan S, et al. Mutations associated with acquired resistance to PD-1 blockade in melanoma. N Engl J Med 2016;375:819–29.
21. Gettinger S, Choi J, Hastings K, Truini A, Datar I, Sowell R, et al. Impaired HLA Class I antigen processing and presentation as a mechanism of acquired resistance to immune checkpoint inhibitors in lung cancer. Cancer Discov 2017;7:1420–35.
22. Sade-Feldman M, Jiao YJ, Chen JH, Rooney MS, Barzily-Rokni M, Eliane JP, et al. Resistance to checkpoint blockade therapy through inactivation of antigen presentation. Nat Commun 2017;8:1136.
23. Porgador A, Mandelboim O, Restifo NP, Strominger JL. Natural killer cell lines kill autologous beta2-microglobulin-deficient melanoma cells: implications for cancer immunotherapy. Proc Natl Acad Sci U S A 1997;94:13140–5.
24. Wagner AK, Wickström SL, Tallerico R, Salam S, Lakshmikanth T, Brauner H, et al. Retuning of Mouse NK Cells after Interference with MHC Class I sensing adjusts self-tolerance but preserves anticancer response. Cancer Immunol Res 2016;4:113–23.
25. Shifrin N, Raulet DH, Ardolino M. NK cell self tolerance, responsiveness and missing self recognition. Semin Immunol 2014;26:138–44.
26. Anfossi N, André P, Guia S, Falk CS, Roetynck S, Stewart CA, et al. Human NK cell education by inhibitory receptors for MHC class I. Immunity 2006; 25:331–42.
27. Nuñez SY, Ziblat A, Secchiari F, Torres NI, Sierra JM, Raffo Iraolagoitia XL, et al. Human M2 macrophages limit NK cell effector functions through secretion of TGF-β and engagement of CD85j. J Immunol 2018;200:1008–15.
28. Noy R, Pollard JW. Tumor-associated macrophages: from mechanisms to therapy. Immunity 2014;41:866.
29. Kaneda MM, Messer KS, Ralainirina N, Li H, Leem CJ, Gorjestani S, et al. PI3Kγ is a molecular switch that controls immune suppression. Nature 2016;539:437–42.